Reac Kinet Mech Cat (2017) 122:655–670
DOI 10.1007/s11144-017-1200-4

# Kinetic study of photocatalytic degradation of the emerging contaminant bisphenol A using N–$TiO_2$ in visible light: a study of the significance of dissolved oxygen

**D. López-Serna[1] · S. I. Suárez-Vázquez[1] · J. C. Durán-Álvarez[2] · R. Zanella[2] · V. H. Guerra-Cobián[1] · A. Cruz-López[1]**

Received: 31 March 2017 / Accepted: 2 June 2017 / Published online: 11 July 2017


**Abstract** This study compares the tracking of bisphenol A (BPA) degradation by three analytical techniques: liquid chromatography mass spectrometry (HPLC–MS), ultraviolet/visible (UV–Vis) spectroscopy and dissolved oxygen (DO) content. In each evaluation method, the photochemical behavior of $TiO_2$ and N–$TiO_2$ under visible light confirmed the relationship between the adsorption and photodegradation processes, with the reaction analysis indicating the possibility of two photocatalytic mechanisms: conventional photocatalyzed radical oxidation and lattice oxygen driven oxidation. The first one concerns HPLC, where the average half-lives ($t_{1/2}$) were 38 min (5% N–$TiO_2$), 60 min (1% N–$TiO_2$) and 64 min ($TiO_2$), these values vary in 12% if compared with the values obtained by UV–Vis spectroscopy. The second mechanism showed a decrease in the initial concentration by more than 50% (8 mg $L^{-1}$) after 3 h. The solution of doped photocatalysts is tracked best by DO measurement. The results presented here confirm that the efficiency of photocatalytic oxidation (EPO) of a reaction is highly related to the DO content, given that dissolved $O_2$ proactively causes the release of radicals on the surface of excited materials under the action of visible light, thus increasing the BPA degradation rate. The quantum yield of BPA disappearance was below 0.1 for all the materials.

**Electronic supplementary material** The online version of this article (doi:10.1007/s11144-017-1200-4) contains supplementary material, which is available to authorized users.

✉ A. Cruz-López
cruz_lopeza@yahoo.com.mx

[1] Universidad Autónoma de Nuevo León, Facultad de Ingeniería Civil, Av. Universidad s/n, Cd. Universitaria, 66455 San Nicolás de los Garza, NL, México

[2] Centro de Ciencias Aplicadas y Desarrollo Tecnológico, Universidad Nacional Autónoma de México, Circuito exterior S/N, Cd. Universitaria, Delegación Coyoacán, Apartado Postal 70-186, C.P. 04510 Ciudad de México, Mexico

**Keywords** Semiconductor · Photocatalysis · Endocrine disrupting · Surface mechanism

## Introduction

Water quality has deteriorated globally, and the preservation of clean water is one of the most important topics worldwide [1]. Nowadays, various toxic organic and inorganic compounds have been detected at critical levels in waste, ground and surface water [1]. At the same time, epidemiological studies have reported the increasing presence of endocrine disruptors in the environment and their potential role in the incidence of metabolic diseases [2–4]. Both of these reasons justify the complete removal of this type of substance from water using tertiary treatments, which has led to the development of various biochemical, electrochemical, sonochemical and membrane processes, as well as photochemical reactions [5].

Photocatalytic processes based on the use of $TiO_2$ or its combination with other materials having improved properties under solar irradiation can be considered a sustainable and energy-efficient solution [6–11]. However, it is necessary to involve other parameters in the process, such as DO concentration, water temperature and the wide variety of compounds existing in the water, and accurate results are required for the large-scale application of this technology. Tracking a reaction with DO is a feasible and reliable alternative, as oxygen plays a key role in photocatalytic reactions by inducing simultaneous oxidation and reduction processes [6, 8].

It is well known in heterogeneous photocatalysis that reactions should be preferentially carried out with a steady, external supply of air, but currently, the cost of aeration in treatment plants represents more than 60% of the operation expense for the entire process, without considering the environmental impact from energy consumption [12]. However, it is necessary to ensure that the $O_2$ concentration does not become the rate-limiting factor. The presence of oxygen has three major roles in photocatalysis [8, 9]. The first is associated with semiconductor excitation (e.g. N–$TiO_2$) and the resulting oxygen reduction, which facilitates the separation of electron–hole charges ($e^-$, $h^+$). In the second role, $O_2$ accepts electrons generated on the $TiO_2$ surface and is reduced to $O_2^-$, $H_2O_2$, OH radicals and Ti–O. These active elements on the material surface promote the photocatalytic oxidation of organic compounds. Finally, during oxidation, $O_2$ combines with organic radicals, which are generated by a reaction between the holes and the reactant, producing oxygen adduct intermediates, such as organoperoxy radicals [6, 8].

The aim of this paper is to show that the monitoring of DO is an alternative for tracking BPA degradation in water treatment plants that use $TiO_2$ and N–$TiO_2$ (N = 1 and 5 wt%) photocatalysts under visible light. For this purpose, a kinetic study was undertaken on photocatalyst performance during the photocatalytic BPA reaction, with measurements taken using different spectrophotometric methods (HPLC and UV–Vis) and a dissolved $O_2$ probe.

## Experimental

### $TiO_2$ preparation

$TiO_2$ was synthesized using a modified sol–gel method, in accordance with the procedure reported elsewhere [10]. To obtain nanostructured $TiO_2$ spheres, a hydrolysis process was used, where 1 mL of tetrabutylorthotitanate (TNBT, Fluka, 97%) was mixed with 100 mL of ethylene glycol (EG, Fisher) in an inert environment ($N_2$) to avoid effects of humidity during hydrolysis. This solution was magnetically stirred for 20 h at room temperature. Then, 98 mL of acetone was mixed with 2 mL of distilled water and added to the first solution to precipitate the $TiO_2$ nanoparticles. The $TiO_2$ nanoparticles were washed and re-dispersed in an ultrasonic bath of ethanol/water (1:1 v/v) solution. This process was repeated twice, followed by centrifugal separation to remove excess ethylene glycol from the surface of the particles. Finally, the material was dried at 80 °C for 16 h and annealed in air at 400 °C for 4 h.

### $TiO_2$ doped with nitrogen

The titanium oxide samples were doped with 1 and 5 wt% nitrogen using the methodology previously reported [10]. This study used melamine as the nitrogen precursor, diluting it with ethylene glycol in an inert environment under vigorous stirring, after which TNBT was added, and the solution was magnetically stirred for 20 h at room temperature. To precipitate the $TiO_2$ nanoparticles, 98 mL of acetone was mixed with 2 mL of distilled water and added to the first solution. The steps for the recovery, washing and annealing of doped $TiO_2$ were similar to those previously performed on $TiO_2$.

### Characterization

The structural properties of $TiO_2$ and $TiO_2$ doped with nitrogen were determined by X-ray diffraction (XRD) using a Rigaku Miniflex diffractometer at a scanning rate of 0.05°/s over a 2θ range of 10–70°. X-ray photoelectron spectroscopy analysis (XPS) was conducted with an Intercovamex XPS 1100 instrument to reveal the presence of dopant in the $TiO_2$ structure. The physical adsorption of $N_2$ at −196 °C was performed using a Quantachrome Autosob-1C analyzer to measure the specific surface areas and adsorption–desorption isotherms [13]. Reflectance spectra of the solids were obtained in air and at room temperature with a Perkin Elmer Lambda 35 UV–Vis spectrophotometer. The bandgap was calculated by measuring the diffuse reflectance of $TiO_2$ using the Kubelka–Munk reflectance transfer model [11]. The total organic carbon was measured using a TOC-VCSN analyzer (Shimadzu).

### Photocatalytic degradation of emerging compound

The photocatalytic activity of the sample was determined by monitoring BPA decomposition at room temperature under visible light. In a dark box, a stirred solution was irradiated with a $GaI_3$ 250 W lamp, which emits visible light (quantum flux at 2886 mmol $m^{-2}$ $s^{-1}$) [14, 15]. The quartz lamp was placed in a refrigerated vessel containing the reactant solution (30 ppm BPA in 200 mL) and 100 mg of photocatalyst. The average pH on the reaction solutions was 5.5 ± 0.2. To achieve saturation of DO and ensure the complete adsorption of BPA onto the semiconductor, a 1 mL $s^{-1}$ flux of dry air was bubbled for 60 min before the light source was turned on. The photocatalytic activity of BPA was calculated from the adsorption band at 275 nm as a function of irradiation time using a Perkin Elmer Lambda 35 UV–vis spectrophotometer. A complementary test for the photochemical reaction of BPA decomposition was conducted by liquid chromatography mass spectrometry (HPLC–MS) using an Agilent Model 6420 system with acetonitrile as the carrier.

### EPO

During the photocatalytic degradation of BPA, the quantum flux was measured with an MQ-200apogee model, and the DO was measured for each material using an Orion 087003 DO probe coupled to a Thermo Scientific Orion Star A325 cell. The evolution of DO was related to the EPO using Eq. 1, as detailed below [16]:

$$E = \frac{\Delta C \times V \times 1000}{I \times s \times t} \tag{1}$$

Here $E$ is the efficiency of photocatalytic oxidation (mg $W^{-1}$ $h^{-1}$), $C$ is the demand for dissolved oxygen ($C^{\circ} = 8.20$ mg $L^{-1}$), $V$ is the solution volume (0.2 $L^{-1}$), I corresponds to the irradiation (0.0684 Mw $cm^{-2}$), $s$ is defined as the irradiated surface (65.9 $cm^2$), and $t$ is the exposition time (h).

### Quantum yield

The disappearance quantum yield was calculated according with the methodology of [17] with the assumption that the optical density in the medium is low, the decrease in light intensity thereby negligible and the average wavelength is 410 nm [17]. The quantum yield (Φ) is defined as the ratio between the number of reacted molecules per unit time and unit volume (in this case see Eq. 4) and the total number of photons absorbed per unit time and unit volume:

$$\Phi = \frac{\text{Number of reacted molecules}}{\text{Number of absorbed photons}} \tag{2}$$

The parameters calculated for total amount of absorbed photons $I_a$, at overage wavelength 410 nm and for time t (s) were then: $I_0$, the intensity of the incoming light (mol $L^{-1}$ $s^{-1}$), $I$ the outgoing light intensity (mol $L^{-1}$ $s^{-1}$), $\varepsilon_\lambda$ the molar

absorption coefficient, (L $mol^{-1}$ $cm^{-1}$), $l$ is the cell path length (cm) and C the concentration of BPA (mol $L^{-1}$).

$$I_{a,\lambda} = tI_{0,\lambda}\left(1 - e^{-2.303\varepsilon_\lambda lC}\right) \quad (3)$$

## Results and discussion

### Physicochemical characterization

*XRD*

Fig. 1 shows the XRD analysis results of both $TiO_2$ and $TiO_2$ doped with nitrogen, prepared by the modified sol–gel method and annealed at 400 °C for 4 h. The diffractogram confirmed the presence of anatase crystals with an orthorhombic structure, whose characteristic reflections were recorded at angles of $2\theta = 25.73$, 37.54, 38.44, 39.10, 48.45, 54.78, 56.01, 63.13, 63.81, and 70.01°, according to card COD-96-101- 0943. There is no evidence of major structural changes in the doped materials given that the $TiO_2$ reflections are the same; however, the level of crystallinity was affected, as evidenced by an increase in the peak width of the 5% N–$TiO_2$ material a trend that has been reported by other authors [18–20]. A detailed description of those diffractograms is given in Fig. S1 of the supplemental material.

*XPS spectroscopy*

Fig. S2 (supplementary material) shows the XPS results for $TiO_2$ and $TiO_2$ doped with nitrogen (1% N–$TiO_2$ and 5% N–$TiO_2$), which was prepared by the modified

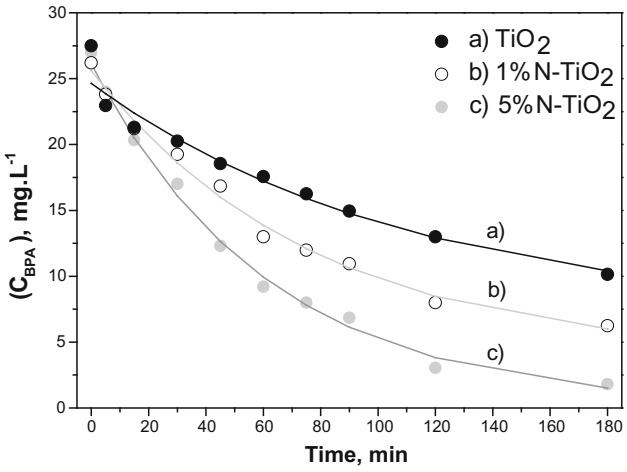


**Fig. 1** The experimental data and non-linear squares model (*solid lines*) for the BPA photodegradation using different photocatalysts of $TiO_2$ and $TiO_2$ doped with nitrogen under action of visible light analyzed by UV–Vis spectroscopy at room temperature. $[C_{BPA0}] = 30$ mg $L^{-1}$, V = 0.2 $L^{-1}$, $m_{catalyst} = 100$ mg

sol–gel method and annealed at 400 °C. Three regions in the XPS spectra were examined: the N 1 s region at approximately 400 eV (Fig. S2-I), the Ti 2p region at approximately 458 eV (Fig. S2-II), and the O 1 s region at approximately 532.5 eV (Fig. S2-III). There are important differences in these three regions among the synthetized materials. The binding energy peak for N 1 s is greater than the typical binding energy for TiN (397.2 eV), and therefore, could be associated with interstitial nitrogen in the form of $NO_x$ [21, 22], which causes defects between the valence band and conduction band [23].

Other authors have reported that nitrogen impurities can induce the excitation of electrons in the bandgap, thus forming a new adsorption band [24, 25]. The Ti 2p signal for non-doped $TiO_2$ was found at 1.2 eV below the assigned binding energy for $TiO_2$. This shift is probably attributed to trace carbon from the synthesis method. Meanwhile, a clear shift toward lower binding energy was observed for the doped materials, indicating the successful incorporation of nitrogen into the $TiO_2$ lattice [7, 22]. Finally, the three samples show O 1 s peaks at 529 eV, related to structural oxygen, and 532 eV, corresponding to oxygen adsorbed on the surface [26].

*UV–Vis spectroscopy*

The bandgap of both $TiO_2$ and $TiO_2$ doped with nitrogen was measured using the diffuse reflectance technique, after which an adjustment was performed by means of the Kubelka–Munk equation, as reported in a previous paper [10].

According to the results shown in Table 1, a 3.2 eV bandgap was observed for $TiO_2$, which corresponds to reports in the literature [7, 10, 27]. The doped solid samples of 1% N–$TiO_2$ and 5% N–$TiO_2$ presented a significant bandgap shift in proximity to the visible region ($\sim$3.05 eV), showing similar behavior to the non-doped sample.

*Nitrogen physisorption*

Table 1 summarizes the surface area results for the materials with an anatase crystalline structure prepared using the modified sol–gel method. It is observed that while $TiO_2$ showed a specific surface area of 60 $m^2\ g^{-1}$, it was slightly modified to 56 $m^2\ g^{-1}$ when nitrogen was added to the structure, constituting a variation of less than 10%. On the other hand, for the 5% N–$TiO_2$ sample, the specific surface area

**Table 1** Surface properties of $TiO_2$ and N-$TiO_2$ prepared by modified sol–gel method at ambient temperature and annealed at 400 °C during 4 h

| Analysis | Sample | | |
|---|---|---|---|
| | $TiO_2$ | 1% N–$TiO_2$ | 5% N–$TiO_2$ |
| Specific surface area $m^2\ g^{-1}$ | 61 | 56 | 120 |
| Pore volume ($cm^3\ g^{-1}$) | 78 | 82 | 108 |
| Bandgap, eV | 3.20 | 3.15 | 3.10 |

was twice that of the other samples. The modification of the morphology and porosity of the $TiO_2$ nanoparticles [6, 18, 26] caused these variations.

The adsorption and desorption isotherms for the materials used in this study are Type IV, as shown in Fig. S3. This type of isotherm is characteristic of mesoporous solids, in which the adsorption is produced in multilayers and reflected in a central zone of the ascending isotherm to the extent that more layers are adsorbed onto the solid surface, clearly describing the surface changes (desorption) that exist in the doped materials, as shown in the hysteresis of the material.

## Photocatalytic activity of emerging compound

### *UV–Vis spectroscopy*

This paper measured the performance of $TiO_2$ and $TiO_2$ doped with nitrogen using a modified sol–gel method during the photocatalytic degradation of BPA under visible light. Fig. S4 shows the evolution of the UV–Vis spectrum during the photocatalytic degradation of BPA in a 30 ppm solution over 180 min. The presence of a maximum peak in the adsorption band of BPA at 275 nm is clearly visible, which has been reported by other authors as well [27, 28]. The figure clearly shows that the spectral intensity decreases along with the contact time of the catalyst in visible light, which is evidence of BPA degradation.

Fig. 1 shows the photocatalytic behavior an increase in the activity of 60% of $TiO_2$ after 180 min of exposure to visible light is observed with similar trend when 1% N–$TiO_2$ (78%) is used. Nevertheless, the most active catalyst is 5% N–$TiO_2$ (90%) reached after 120 min of reaction. On the other hand, Fig. 1 shows the calculation of kinetic parameters calculated by exponential model showed in Eq. 4 [29–31].

$$g(t) = Xe^{-kt} + E \tag{4}$$

In this equation, X is the concentration of [BPA] at different times (mg $L^{-1}$), k is the first order rate constant ($min^{-1}$), whereas E is called the endpoint of the process (mg $L^{-1}$). According with non-linear model for the BPA photodegradation, the rate constants reaction were calculated for the different catalyst obtaining the next results $k_{5\%\ \text{N-TiO2}} = 0.0162\ min^{-1}$, $k_{1\%\ \text{N-TiO2}} = 0.0130\ min^{-1}$ and $k_{TiO2} = 0.0090\ min^{-1}$. The calculated half-lives values are $t_{1/2} = 43$, 53 and 76 min for 5% N–$TiO_2$, 1% N–$TiO_2$ and $TiO_2$. It is worth mentioning that although the regression coefficients were around 0.9881, the three experimental data showed that the standard deviations were not significant being located in the range $0.0011 < \sigma_k < 0.0023$ (see Table 2) [31].

### *DO measurement*

During the BPA degradation reaction described above, the DO consumption was analyzed, as described in the experimental section. Fig. 2a shows the photolysis of the BPA solution, which did not present any variation over the 3 h interval. With the

**Table 2** Percentage of TOC removal and kinetic parameters of BPA photodegradation under visible light using $TiO_2$ and N–$TiO_2$ prepared by modified sol–gel method

| Analyses | Units | Samples | | |
|---|---|---|---|---|
| | | $TiO_2$ | 1% N–$TiO_2$ | 5% N–$TiO_2$ |
| UV–Vis spectroscopy | K ($min^{-1}$) | 0.0090 ± 0.0023 | 0.0130 ± 0.0014 | 0.0162 ± 0.0011 |
| | $t_{1/2}$ (min) | 76 | 53 | 43 |
| | X (mg $L^{-1}$) | 17.6832 ± 2.2786 | 21.7088 ± 1.0128 | 26.0222 ± 0.7561 |
| | E (mg $L^{-1}$) | 6.9551 ± 2.4480 | 3.9062 ± 1.0813 | 0.1130 ± 0.7754 |
| | $R^2$ | 0.9758 | 0.9927 | 0.9959 |
| HPLC–MS spectroscopy | k ($min^{-1}$) | 0.0108 ± 0.0039 | 0.0114 ± 0.0129 | 0.0181 ± 0.0015 |
| | $t_{1/2}$ (min) | 64 | 60 | 38 |
| | X (mg $L^{-1}$) | 16.0261 ± 2.7415 | 25.066 ± 15.7570 | 26.4540 ± 0.9970 |
| | E (mg $L^{-1}$) | 9.9802 ± 2.9557 | 1.9296 ± 10.9650 | 1.2893 ± 0.8800 |
| | $R^2$ | 0.9937 | 0.9836 | 0.9379 |
| Dissolved oxygen | $K_{OD}$ ($min^{-1}$) | 0.0038 | 0.0044 | 0.1023 |
| | $1/r_{maxOD}$ (mg $L^{-1}$)$^{-1}$ | 0.0004 ± 0.0277 | 0.0017 ± 0.0019 | 0.0731 ± 0.0012 |
| | $R^2$ | 0.9964 | 0.9998 | 0.9997 |
| | $1/r_{OD}$ (mg $L^{-1}$)$^{-1}$ | 0.0035 | 0.0610 | 0.1000 |
| TOC removal (3 h) | % | <50 | <50 | >85 |

addition of catalysts to the three materials, a greater consumption of DO was noted, with the highest consumption for the 5% N–$TiO_2$ sample of 4 mg $L^{-1}$ in the first hour. For 1% N–$TiO_2$, the same level of oxygen consumption took 120 min, while finally, the $O_2$ consumption of the non-doped $TiO_2$ photocatalyst was very slow, recording a total consumption of less than 2.5 mg $L^{-1}$ over the entire reaction time. The photocatalytic stability was also measured during the BPA degradation reaction using 5% N–$TiO_2$, as shown in Fig. 2b. This figure shows that the catalytic activity is the same after two cycles, it means the rate of $O_2$ evolution in the second run with intermittent evacuation was unchanged compared to the first run, and the reaction continued to proceed steadily with consume of oxygen around 85%.

Equation 3 represents the conventional Langmuir–Hinshelwood mechanism.

$$\frac{1}{r_{OD}} = \frac{1}{r_{\mathrm{maxOD}}} + \frac{1}{r_{\mathrm{maxOD}} K_{OD}[O2]} \tag{5}$$

Here $r_{max}$ is the maximum DO consumption and $K_D$ is the equilibrium constant for the adsorption reaction. When the adsorption sites are fully occupied by reactant molecules, $r_{max}$ is equivalent to $r_{DO}$ [8].

By plotting the inverse of the DO decay concentration against the inverse of the time (see Fig. 2c). A linear relationship can be detected among the different materials; nevertheless, $r_{maxOD}$ and the apparent constant of the material tends to approach zero as the nitrogen content decreases ($K_{5\%\ N\text{–}TiO2} = 0.1023\ min^{-1} > K_{1\%\ N\text{–}TiO2} = 0.0044\ min^{-1} > K_{TiO2} = 0.0038\ min^{-1}$), as shown in Table 2. The

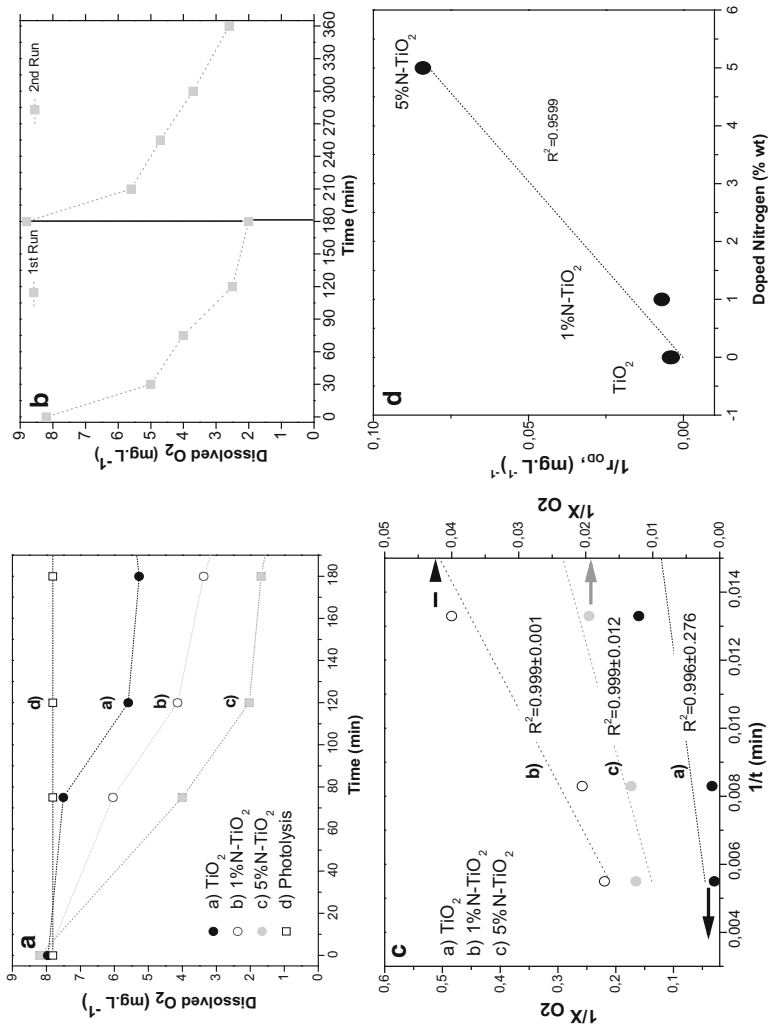


**Fig. 2** Evolution of DO consumption during photodegradation reaction of BPA using different photocatalysts of $TiO_2$ and $TiO_2$ doped with nitrogen under action of visible light. $[C_{O2,0}] = 8$ mg $L^{-1}$, $V = 0.2$ $L^{-1}$, $m_{catalyst} = 100$ mg. **a** DO $O_2$ vs. time, **b** 5%N-$TiO_2$, **c** 1/t vs. $1/[X_{O2\ Dissolved}]$, **d** Kinetic model of Langmuir Hishelwood for DO

regression coefficients were around 0.999 for the doped materials nevertheless the three experimental data showed that the standard deviations were not significant being located in the range $0.276 < \sigma_k < 0.001$ (see Table 2). The adjustment of the apparent constants using the Langmuir–Hinshelwood kinetics model is shown in Fig. 2d. This image agrees with previous reports [8, 32]. The kinetic parameters for the less active materials tend to approach zero ($1/r_{OD} < 0.0610$ (mg $L^{-1})^{-1}$) reflecting the worse adsorption equilibrium of photocatalysis, while the doped material 5% N–$TiO_2$ [$1/r_{OD} = 0.1$ (mg $L^{-1})^{-1}$] presented the best availability to adsorb oxygen produced by oxygen vacancies generated by nitrogen doping [8].

DO measurements can also be used to define the EPO in contact with the solution per watt of energy (see Eq. 1) as shown in Fig. 3. The 5% N–$TiO_2$ photocatalyst attained the best performance (150 W $mg^{-1}$ $L^{-1}$) in the first 60 min of reaction, while 1% N–$TiO_2$ and $TiO_2$ were less sensitive to optical phenomena and reached their maximum value in the second hour, recording 90 and 59 W $mg^{-1}$ $L^{-1}$, respectively. These behaviors correspond to the BPA degradation reaction observed using UV–Vis spectroscopy, the results of which are described above. These results show that a 50% reduction in BPA concentration occurs after 60 min of reaction using the 5% N–$TiO_2$ photocatalyst.

Table 3 shows the quantum yields of BPA disappearance under visible light using $TiO_2$ and N–$TiO_2$ prepared by modified sol–gel method. No major differences between the disappearance quantum yield of $TiO_2$ and 1% N–$TiO_2$ at pH 5.5 were observed, while the disappearance quantum yield of 5% N–$TiO_2$ was two times higher. That value are according with previous reports for BPA [15].

At this point, it is necessary to compare the relationship between the adsorption and photodegradation processes, as the reaction analysis indicates the possibility of two photocatalytic mechanisms: conventional photocatalyzed radical oxidation and lattice oxygen driven oxidation [33, 34]. The former involves the formation of both

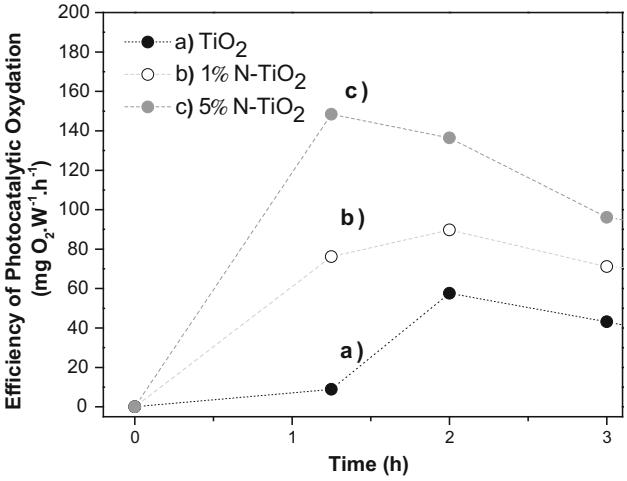


**Fig. 3** EPO of $TiO_2$ and $TiO_2$ doped with nitrogen during photocatalytic degradation of BPA using visible light ($GaI_3$, 250 W), $[C_{A0}] = 30$ mg $L^{-1}$, V = 0.2 $L^{-1}$, $m_{catalyst} = 100$ mg

**Table 3** Quantum yields of BPA disappearance under visible light using $TiO_2$ and N–$TiO_2$ prepared by modified sol–gel method. $\lambda = 410$ nm, $t = 3600$ s, $l = 2.5$ cm

| Sample | Coming light intensity, $I_{o,\lambda}$ (mol $L^{-1}$ $s^{-1}$) | Outgoing light intensity, $I$ (mol $L^{-1}$ $s^{-1}$) | $[C_{BPA}]$ mol $L^{-1}$ | Molar absorption coefficient, ε L $mol^{-1}$ $cm^{-1}$ | Number of absorbed photons ($I_{a,\lambda}$) | Number of reacted molecules (L $mol^{-1}$ $cm^{-1}$) | Quantum yield |
|---|---|---|---|---|---|---|---|
| $TiO_2$ | 0.087 | 0.006 | 6.30E-05 | 7135.860 | 289.716 | 10 | 0.035 |
| 1% N–$TiO_2$ | 0.087 | 0.024 | 4.78E-05 | 4650.3820 | 226.225 | 14 | 0.061 |
| 5% N–$TiO_2$ | 0.087 | 0.034 | 3.42E-05 | 4717.227 | 189.691 | 18 | 0.096 |

$h^+$ and ·OH species on the surface of the catalyst, which are associated with the reduction of DO during the photocatalytic process [9], while in the solid phase, the structural and optical properties play an important role in the bandgap [30]. In addition, the amphoteric character of $TiO_2$ can lead to a change in the concentration of $H^+$ and $OH^-$ when nitrogen is added, thus modifying the surface charge [35]. A negative charge on the surface indicates that cationic BPA ions have been efficiently adsorbed on the surface [35, 36].

*HPLC–MS*

Fig. 4 shows the evolution over time of BPA conversion using doped and non-doped titanium oxides. The results obtained with this technique show similar behavior to the photocatalytic assays analyzed with UV–Vis spectroscopy. The 5% N–$TiO_2$ photocatalyst achieved conversions greater than 90% after 3 h of light exposure. This was followed by the 1% N–$TiO_2$ photocatalyst, which reached a conversion level of 80% over the same time period, and finally, by $TiO_2$, with a conversion of 65%.

The kinetic non-linear model summarized in Table 2 corroborates that the different photocatalysts present a behavior with rate constants of $k_{5\%\ N\text{–}TiO2} = 0.0181\ min^{-1}$, $k_{1\%\ N\text{–}TiO2} = 0.0114\ min^{-1}$ and $k_{TiO2} = 0.0108\ mg\ L^{-1}\ min^{-1}$. The average half-lives obtained are $t_{1/2} = 38$ min, $t_{1/2} = 60$ min and $t_{1/2} = 64$ min for 5% N–$TiO_2$, 1% N–$TiO_2$ and $TiO_2$, respectively. The regression coefficients were around 0.9724.

Table 2 confirms that the percentage of TOC removal for the 5% N–$TiO_2$ sample was >85% after 3 h. All samples reached complete mineralization after 24 h. These

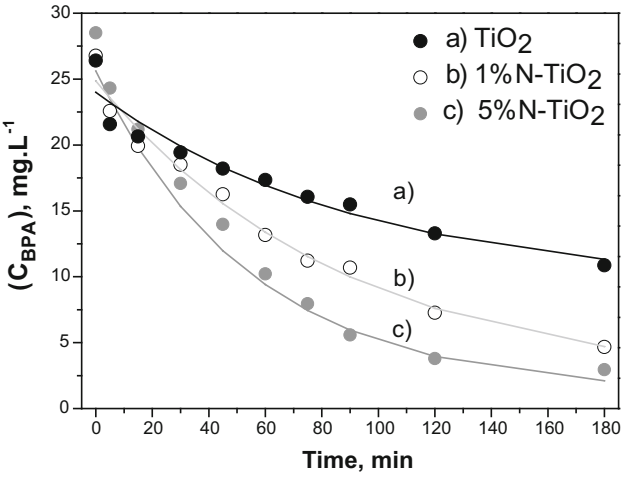


**Fig. 4** The experimental data and non-linear squares model (*solid lines*) for the BPA photodegradation using different photocatalysts of $TiO_2$ and $TiO_2$ doped with nitrogen under action of visible light using HPLC–MS equipment. $[C_{BPA0}] = 30\ mg\ L^{-1}$, $V = 0.2\ L^{-1}$, $m_{catalyst} = 100$ mg

efficiencies were comparable with the results for materials reported by Subagio [35], which had similar surface areas. While the identification of intermediates produced by the oxidation reaction is beyond the scope of this study, some mechanisms have been proposed for the photocatalytic degradation of BPA. According to the literature, the reaction could be initiated by ·OH attacking the electron-rich $C_3$ in the phenyl group [35, 37]. This reaction is followed by the cleavage of the phenyl group into 4-isopropanolphenol, 4-isopropylphenol, 4-isopropenylphenol or 4-hydroxy-acetonphenol, either sequentially or directly through the formation of transient intermediates or radicals [$^{\bullet}H$ and $^{\bullet}C(CH_3)_2C_6H_4OH$)]. In addition, immediate ring cleavage caused by $OH^-$ attacking BPA to form 3-hydroxy-1,3,5-hexadiene has been previously proposed for N–$TiO_2$ [35, 37]. However, according to CAS, in all cases, the byproducts are non-toxic [38].

Table 2 shows a summary of the kinetic constants and the half-lives of BPA degradation during the photocatalytic assays analyzed by UV–Vis spectroscopy and HPLC–MS. The rate constants show a negligible difference between the most active samples identified by both analyses (less than 10%). However, at lower degradation values, the difference is more sensitive for HPLC–MS analysis, which identified a value 10% smaller than that obtained by UV–Vis spectroscopy. This difference is probably due to the higher perturbation of the optical phenomena.

Finally, Fig. 5 shows the concentration profile of BPA, as identified by HPLC–MS, UV–Vis spectroscopy and DO content over time, using the 5% N–$TiO_2$ photocatalyst under visible light. This figure reveals similar behavior regardless of the measurement method, which can be considered good evidence that degradation reactions can be tracked by measuring the DO content.

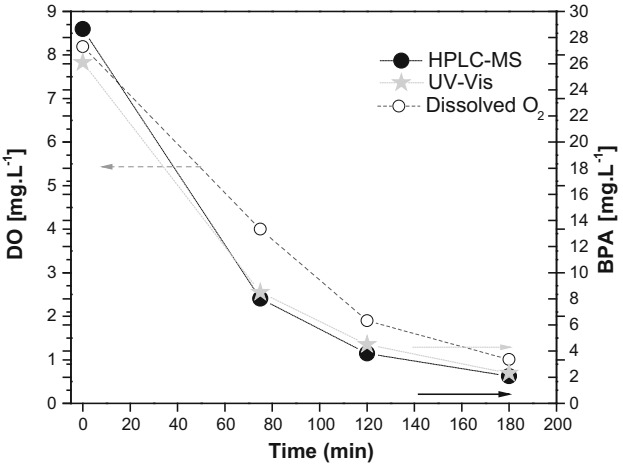


**Fig. 5** Evolution profile of BPA degradation and DO on 5% N–$TiO_2$ catalyst analyzed by UV–Vis spectroscopy, HPLC–Ms and $O_2$. $[C_{A0}] = 30$ mg $L^{-1}$, $[O_{2,0}] = 8$ mg $L^{-1}$, $V = 0.2$ $L^{-1}$, $m_{catalyst} = 100$ mg

## Conclusion

The physicochemical characterization of the materials, prepared with a modified sol–gel method and annealed at 400 °C, shows the resulting $TiO_2$ to be in the anatase phase with a specific surface area of 60 $m^2\ g^{-1}$ and a bandgap of 3.2 eV. These properties are modified, enhancing their activation in the visible region, with the addition of 1 and 5% of nitrogen.

Tracking BPA degradation by three different methods (UV–Vis spectroscopy, HPLC–MS and dissolved oxygen content) showed non-significant standard deviations in the range ($0.0011 < \sigma_k < 0.0023$ and $0.0015 < \sigma_k < 0.0039$) for UV–Vis spectroscopy and HPLC–MS. After the adjustment of the spectrophotometer results to a kinetic model, the photocatalysts showed the following average half-lives: 38 min (5% N–$TiO_2$), <60 min (1% N–$TiO_2$) and <64 min ($TiO_2$).

The Langmuir–Hinshelwood model showed the ability of BPA adsorption on the surface (5% N–$TiO_2$), which improve the rate of reaction for dissolved $O_2$.

The results presented here confirm that the quantum efficiency of a reaction is highly related to the dissolved oxygen content, given that dissolved $O_2$ proactively causes the release of radicals on the surface of excited materials under the action of visible light, thus increasing the BPA degradation rate.

Measurement of the DO concentration was implemented as an alternative for confirming BPA mineralization, leading to the observation that the presence of oxygen is a key factor in the development of an advanced oxidation process, such as heterogeneous photocatalysis. Although the use of semiconductor material causes activity in the visible region of the electromagnetic spectrum, it is important to measure and maintain the DO concentration to assure complete mineralization.

**Acknowledgements** DLS wishes to thank CONACyT for the financial support (Master and mixed scholarship). Dr. Santiago I. Suárez are gratefully acknowledged for valuable support of PROMEP Nuevo PTC DSA/103.5/16/10510. R. Zanella acknowledges the financial support granted by PAPIIT 105416, UNAM, Mexico. Authors thank to PAICYT IT 404-15 and IT 510-15. The authors thank the Materials' Laboratory of Facultad de Ingenieria Civil-UANL for allowing them to perform the described experiments.

## References

1. Bhatnagar A, Sillanpäa M, Witek-Krowrak A (2015) Agricultural waste peels as versatile biomass for water purification—a review. Chem Eng J 270:244–271
2. Lorber M, Schecter A, Paepke O, Shropshire W, Christensen K, Birnbaum L (2015) Exposure assessment of adult intake of bisphenol A (BPA) with emphasis on canned food dietary exposures. Environ Inter 77:55–62
3. Carlson JC, Stefan MI, Parnis JM, Ch D (2015) Direct UV photolysis of selected pharmaceuticals, personal care products and endocrine disruptors in aqueous solution. Water Res 84:350–361
4. Chao-Yin K, Chung-Hsin W, Jui-Tai W, Yu-Ren C (2015) Synthesis and Characterization of a phosphorus-doped $TiO_2$ immobilized bed for the photodegradation of bisphenol A under UV and sunlight irradiation. Reac Kinet Mech Cat 114:453–766
5. Kralchevska R, Milanova M, Bistan M, Pintar A, Todorovsky D (2013) Photocatalytic degradation of some endocrine disruptin compounds by modified $TiO_2$ under UV or halogen lamp illumination. Reac Kinet Mech Cat 109:355–373

6. Turchi CS, Ollis DF (1990) Photocatalytic degradation of organic water contaminants: mechanisms involving hydroxyl radical attack. J Catal 122(1):178–192
7. Manzo-Robledo A, Cruz López A, Flores Caballero AA, Zaldivar Cadena AA, López M, Vázquez Cuchillo O (2015) Photoelectrochemical properties of sol–gel synthesized titanium dioxide nanoparticles using different acids: X-ray photoelectron spectroscopy reveals the induced effect of hydrolysis precursor. Mater Sci Semi Proc 31:94–99
8. Hirakawa T, Koga C, Negishi N, Takeuchi K, Matsuzawa S (2009) An approach to elucidating photocatalytic reaction mechanisms by monitoring dissolved oxygen: effect of $H_2O_2$ on photocatalysis. Appl Catal B 87:46–55
9. García-Fernández I, Fernández-Calderero I, Polo-López MI, Fernández-Ibañez P (2015) Disinfection of urban effluents using solar $TiO_2$ photocatalysis: a study of significance of dissolved oxygen, temperature, type of microorganism and water matrix. Catal Today 240:30–38
10. Del Ángel-Sánchez K, Vázquez-Cuchillo O, Salazar-Villanueva M, Sánchez Ramírez JF, Cruz-López A, Aguilar-Elguezabal A (2011) Preparation, characterization and photocatalytic properties of TiO2nanostructured spheres synthesized by the Sol-Gel method modified with ethylene glicol. J Sol–Gel Sci Technol 38:360–365
11. Yunjin Y, Jiacheng Q, Chen H, Fengyu W, Xueting L, Jianlong W, Shaobin W (2015) one-pot approach for synthesis of N-doped $TiO_2/ZnFe_2O_4$ hydbrid as an efficient photocatalyst for degradation of aqueous organic pollutants. J Hazard Mater 291:28–37
12. Pablo-Romero MP, De Jesús J (2016) Economic growth and energy consumption: the Energy-Environmental Kuznets Curve for Latin America and the Caribbean. Renew Sustain Energy 60:1343–1350
13. Zhang YZ, Song XF, Kondoh A, Xia J, Tang ChY (2011) Behavior, mass inventories and modeling evaluation of xenobiotic endocrine-disrupting chemicals along an urban receiving wastewater river in Henan Province, China. Water Res 45:292–302
14. Kitsinelis S, Zissis G, Fokitis E (2009) A strategy towards the next generation of low pressure discharge lamps: lighting after mercury. J Phys D 42:1–8
15. Klauson D, Gromyko I, Dedova T, Pronina N, Krichevskaya M, Budarnaja O, Oja Acik I, Volobujeva O, Sildos I, Utt K (2015) Study on photocatalytic activity of ZnO nanoneedles, nanorods, pyramids and hierarchical structures obtained by spray pyrolysis method. Mater Sci Semi Proc 31:315–324
16. Del Ángel-Sanchez K, Vázquez-Cuchillo O, Aguilar-Elguezabal A, Cruz-López A, Herrera-Gómez A (2013) Photocatalytic degradation of 2,4-dichlorophenoxyacetic acid under visible light: effect of synthesis route. Mater Chem Phys 139:423–430
17. Ericksson J, Rahm S, Green N, Bergman Å, Jakobsson E (2004) Photochemical transformation of tetrabromobispehnol A and related phenols in water. Chemosphere 54(2004):117–126
18. Xie Y, Zhao X, Li Y, Zhao Q, Zhou X, Yuan Q (2008) CTAB-assisted synthesis of mesoporous F-N-codoped $TiO_2$ powders with high visible-light-driven catalytic activity and adsorption capacity. J Solid State Chem 181:1936–1942
19. Dong F, Zhao W, Wu Z, Guo S (2009) Band structure and visible ligbt photocatalytic activity of multi.type nitrogen doped $TiO_2$ nanoparticles prepared by termal descomposition. J Hazard Mater 162:763–770
20. Di Valentin C, Finazzi E, Pacchioni G, Selloni A, Livraghi S, Paganini MC, Giamello E (2007) N-doped $TiO_2$: theory and experiment. Chem Phys 339:44–56
21. Lee S, Cho I-S, Lee DK, Kim DW, Noh TH, Kwak CH, Park S, Hong KS, Lee J-K, Jung HS (2010) Influence of nitrogen chemical states on photocatalytic activities of nitrogen-doped $TiO_2$ nanoparticles under visible light. J Photochem Photobiol A 213:129–135
22. Chen X, Burda C (2004) Photoelectrons investigation of Nitrogen-doped titania nanoparticles. J Phys Chem B 108:15446–15449
23. Ashi R, Morikawa T, Ohwaki T, Aoki K, Taga Y (2001) Visible-light photocatalysis in nitrogen-doped titanium oxide. Science 239:269–271
24. Barolo G, Livraghi S, Chiesa M, Paganini MC, Giamello E (2012) Mechanism of the photoactivity under visible light of N-doped titanium dioxide. Charge carriers migration in irradiated N-$TiO_2$ investigated by electron paramagnetic resonance. J Phys Chem C 116(39):20887–20894
25. Hoang S, Berglund SP, Hahn NT, Bard AJ, Mullins CB (2012) Enhancing visible light photooxidation of water with $TiO_2$ nanowire arrays via co-treatment with $H_2$ and $NH_3$: synergistic effects between $Ti^{3+}$ and N. J Am Chem Soc 134(8):3659–3662

26. Frontistis Z, Daskalaki VM, Katsaounis A, Poulios I, Mantzavinos D (2011) Electrochemical enhancement of solar photocatalysis: degradation of endocrine disruptor bisphenol-A on Ti/$TiO_2$ films. Water Res 45:2996–3004
27. Hou CH, Huang S-H, Chou PH, Den W (2015) Removal of bisphenol A from aqueous solutions by electrochemical polymerization on a carbon aerogel electrode. J Taiwan Inst Chem Eng 51:103–108
28. Tsai W-T, Lee M-K, Su T-S, Chang YM (2009) Photodegradation of bisphenol-A in a batch $TiO_2$ suspension reactor. J Hazard Mater 168:269–275
29. Levenspiel O (2015) Ingeniería de las reacciones químicas. Limusa, Mexico
30. Lente G (2016) Editorial. React Kinet Mech Cat 119(1):3–4
31. Lente G (2015) Deterministic kinetics in chemistry and systems biology. The dinamics of complex reaction networks. Spinger, Berlin
32. Yanxiang L, Xujie L, Feng W, Nansheng D (2011) Adsorption and photooxidation of pharmaceuticals and personal care products on clay minerals. Reac Kinet Mech Cat 104:61–73
33. Ali AM, Emanuelsson EAC, Petterson DA (2011) Conventional versus lattice photocatalysed reactions: implications of the lattice oxygen participation in the liquid phase photocatalytic oxydation with nanostructired ZnO thin film on reaction products and mechanism at both 254 and 340 nm. Appl Catal B 106:323–336
34. Miyauchi M, Ikezawa A, Tobimatsu H, Irie H, Hashimoto K (2004) Zeta potential and photocatalytic activity of nitrogen doped $TiO_2$ thin films. Phys Chem Chem Phys 6:865–870
35. Subagio DP, Srinivasan M, Lim M, Lim TT (2010) Photocatalytic degradation of bisphenol-A by nitrogen-doped $TiO_2$ hollow sphere in a vis-LED photoreactor. Appl Catal B 95:414–422
36. Zhang X, Ding Y, Tang H, Han X, Zhu L, Wang N (2014) Degradation of bisphenol A by hydrogen peroxide activated with $CuFeO_2$ microparticles as a heterogeneous Fenton-like catalyst: efficiency, stability and mechanism. Chem Eng J 246:251–262
37. Kondrakov AO, Ignatev AN, Lunin VV, Frimmel FH, Bräse S, Horn H (2016) Roles of water and dissolved oxygen in photocatalytic generation of free OH radicals in aqueous $TiO_2$suspensions: an isotope labeling study. Appl Catal B 182:424–430
38. Almeida AR, Moulijn JA, Mul G (2011) Photocatalytic oxydation of cyclohexane over $TiO_2$: evidence for a Mars-van Krevelen mechanism. J Phys Chem C 115:1330–1338